Effect of Bottom Electrode Materials on the Electrical and Reliability Characteristics of (Ba, Sr)TiO_3 Capacitors

Ming Shiahn Tsai, S. C. Sun, and Tseung-Yuen Tseng, *Senior Member, IEEE*

***Abstract*— The dielectric constant and the leakage current density of (Ba, Sr)TiO_3 (BST) thin films deposited on various bottom electrode materials (Pt, Ir, IrO_2/Ir, Ru, RuO_2/Ru) before and after annealing in O_2 ambient were investigated. The improvement of crystallinity of BST films deposited on various bottom electrodes was observed after the postannealing process. The dielectric constant and leakage current of the films were also strongly dependent on the postannealing conditions. BST thin film deposited on Ir bottom electrode at 500 °C, after 700 °C annealing in O_2 for 20 min, has the dielectric constant of 593, a loss tangent of 0.019 at 100 kHz, a leakage current density of 1.9×10^{-8} A/cm^2 at an electric field of 200 kV/cm with a delay time of 30 s, and a charge storage density of 53 fC/μm^2 at an applied field of 100 kV/cm. The BST films deposited on Ir with post-annealing can obtain better dielectric properties than on other bottom electrodes in our experiments. And Ru electrode is unstable because the interdiffusion of Ru and Ti occurs at the interface between the BST and Ru after postannealing. The ten-year lifetime of time-dependent dielectric breakdown (TDDB) studies indicate that BST on Pt, Ir, IrO_2/Ir, Ru, and RuO_2/Ru have long lifetimes over ten years on operation at the voltage bias of 2 V.**

***Index Terms*— (Ba, Sr)TiO_3, electrode, electrical properties, reliability, thin film capacitors.**

I. Introduction

THE advancement of dynamic random access memories (DRAM's) has significantly decreased the available area per cell. Electroceramic thin films with high dielectric constant have attracted great attention for practical use in capacitors of gigabit DRAM's since the adoption of high-dielectric-constant materials can lower the height of the storage node and simplify the cell structure [1]–[4]. One of the most promising materials for the capacitor dielectric films is (Ba,Sr)TiO_3 (BST) because of its high dielectric constant, low leakage current density, high dielectric breakdown strength, paraelectric perovskite phase that does not exhibit fatigue, and the ease of composition control due to the absence of volatile lead oxide [1]–[9].

The electrical characteristics of BST thin films greatly depend on the deposition conditions (sputtering power, substrate temperature, sputtering ambient, gas pressure, etc.) [6], [9]–[11], the composition of the BST thin films [3], [12], the bottom electrode materials, (Pt, Ru, Ir, Pt/Ta, Pt/TiN/Ti, Pd/Ti, Pd, etc.) [13]–[27], and the postdeposition annealing conditions [10], [28]–[30]. Although there is much experimental verification that annealing conditions can have significant effects on the properties of the films, systematic studies of the effect of annealing conditions on the dielectric and electrical properties of BST thin films on various bottom electrodes are still lacking. Integration of ferroelectric capacitors with Si CMOS technology for DRAM and FeRAM applications usually demands several high temperature annealing treatments (>500 °C) which imposes stringent requirements on electrode materials. Among the electrode materials, Pt has a merit of small leakage current density, which is the most studied electrode material for ferroelectric capacitors. However, problems in using Pt in ferroelectric/Si technology such as difficulties in etching, poor adhesion to SiO_2/Si substrate, poor diffusion barrier to oxygen, and high costs have prompted the search for alternative electrode materials. Some transition metal oxides are attractive candidates for electrode materials because of their stability in oxygen ambient at high temperature and metallic conductivity (Table I) [31]. Cho *et al.* have reported that 36-nm-thick ($Ba_{0.5}Sr_{0.5}$)TiO_3 films with the equivalent SiO_2 thickness of 0.4 to 0.5 nm and sufficiently low leakage current of 2×10^{-8} A/cm^2 at 1.5 V were obtained on Ir and IrO_2 electrodes [25]. NEC's researchers have successfully deposited BST thin films on fine-patterned RuO_2, which showed low leakage current and high dielectric constant [19], [20], [23]. Mitsubishi's researchers have also succeeded in obtaining high quality BST thin films on Ru without RuO_2 formation (leakage current of 2×10^{-7} A/cm^2 at 1.5 V) [13]. Advantages gained through the ease of etching Ru may be offset by a higher leakage current [32]. Conducting metal

TABLE I
SOME IMPORTANT PROPERTIES OF CONDUCTIVE TRANSITION METAL OXIDES [31]

	RuO_2	IrO_2	RhO_2	OsO_2	ReO_2
Bulk resistivity ($\mu\Omega$-cm)	40	30	100	60	10
Stability in O_2 ambient	up to 800 °C	up to 1100 °C	up to 850 °C	up to 500 °C	up to 450 °C

Manuscript received July 29, 1998; revised April 20, 1999. The review of this paper was arranged by Editor J. M. Vasi. This work was supported by the National Science Council of R.O.C. under Project NSC 85-2112-M009-037.

The authors are with the Department of Electronics Engineering and Institute of Electronics, National Chiao Tung University, Hsinchu 30050, Taiwan, R.O.C.

Publisher Item Identifier S 0018-9383(99)06647-2.

oxide RuO_2 is perhaps the most widely studied transition metal oxide for electrode material for ferroelectric capacitors [5]. However, IrO_2 has a lower bulk resistivity than RuO_2 (30 $\mu\Omega$-cm versus 40 $\mu\Omega$-cm). IrO_2 and Ir have been used with PZT capacitors to reduce fatigue [33]. It has been shown by previous investigation that BST film capacitors can exhibit excellent electrical characteristics by using Ir as the top electrode [17]. Although there is much experimental proof that bottom electrode materials can significantly affect the properties of the films, systematic studies of the effect of various bottom electrodes during rf sputtering on the electrical and reliability characteristics of BST thin films are still quite limited.

In this work, we have investigated the effects of bottom electrode materials (Pt, Ir, IrO_2/Ir, Ru, RuO_2/Ru) on the dielectric constant and the leakage current density in BST thin films without and with postannealing and propose them as optimum electrode materials. The structural, electrical, and dielectric properties of the films are evaluated and discussed.

II. Experimental

BST thin films were deposited on metals/SiO_2/(100)Si bottom electrodes (metals are Pt, Ir, IrO_2/Ir, Ru, and RuO_2/Ru) by RF magnetron sputtering. The starting p-type silicon wafer was cleaned by a standard RCA cleaning process and chemically etched in a dilute HF solution. The 100-nm thick SiO_2 layer was thermally grown at 1050 °C in a dry oxidation furnace. The metal-layers on SiO_2/Si substrate with a thickness of 100 nm were deposited using a separate RF magnetron sputtering system. The Pt, Ir, and IrO_2 films were prepared at fixed power of 50 W (power density is 2.55 W/cm^2), constant pressure of 5 mtorr, and substrate temperature of 350 °C. The Ru and RuO_2 films were prepared at fixed power of 100 W (power density is 5.1 W/cm^2), constant pressure of 10 mtorr, and substrate temperature of 350 °C. IrO_2 and RuO_2 films were formed by RF magnetron sputtering with Ar and O_2 mixture in the mixing ratio of 4 : 1. The measured resistivities of Pt, Ir, IrO_2, Ru, and RuO_2 were about 17, 27, 67, 228, and 370 $\mu\Omega$-cm at room temperature, respectively.

The BST 50/50 targets with a diameter of 3 in and a thickness of 1/4 in were synthesized using standard solid-state reaction process. The sputtering chamber was evacuated to a base pressure of 2×10^{-6} torr. All films were prepared at fixed power of 100 W (power density is 2.26 W/cm^2) and constant pressure of 10 mtorr which was maintained by a mixture of argon and oxygen at a mixing ratio of 1 : 1 with a total flow of 20 sccm. All of the BST films have the same thickness of around 80 nm. The substrate temperature of the sputtered BST films was at 500 °C. The composition of sputtered films was Ba/Sr = 0.47/0.53 on the basis of ICP analysis. To understand the effect of postannealing, part of the BST thin films after deposition was annealed at temperatures ranging from 500 to 700 °C in O_2 atmosphere using a quartz glass tube furnace (FN) for 20 min. Finally, the 50-nm thick Pt top electrodes with diameters of 165, 255, and 350 μm were formed by sputtering and then patterned by the shadow mask process.

The film thickness was determined from ellipsometry. The structure was characterized by X-ray diffraction (XRD, Siemens D5000). On the basis of XRD data, the average grain size was determined by using Scherrer's formula [6]. The surface roughness and morphology were examined by atomic force microscopy (AFM, Digital Instruments Nano-Scope III). Depth profiles of oxygen near the interface of BST/bottom electrodes were analyzed by secondary ion mass spectrometry (SIMS, CAMECA IMS-4f). The capacitance-voltage (C-V) characteristics were measured on the metal-insulator-metal (MIM) structure by measuring the capacitance at 100 kHz as a function of a swept positive-to-negative voltage bias. Dielectric constant of the films was calculated from the capacitance measured at 100 kHz without bias voltage. The dielectric and loss properties were measured as a function of frequency with a Hewlett-Packard (HP) 4194A impedance gain phase analyzer. The current-voltage (I-V) measurements were performed by measuring the current through the sample with an HP4145B. A Pt top electrode of BST capacitor was connected to the voltage source and the bottom electrode was grounded. The polarity is positive when a positive voltage is applied to the top electrode. All data reported in this paper are the average values of ten specimens. The dielectric constant and leakage current density are independent on the electrode area.

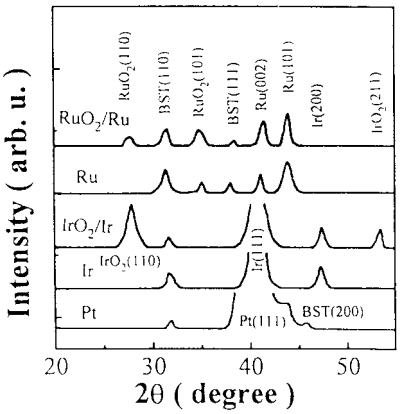

Fig. 1. XRD patterns of BST films deposited at 500 °C on Pt, Ir, IrO_2/Ir, Ru, and RuO_2/Ru bottom electrode materials.

III. Results and Discussion

A. Effect of Bottom Electrodes

The importance of the bottom electrode materials in determining the microstructure of the BST film grown on them is evident from the XRD patterns shown in Fig. 1. The as-deposited BST films exhibit (110) peak for all electrode materials. We note that the (110) peak for the films on Ru and RuO_2/Ru has stronger intensity, while that for the film on Pt reveals fairly weak intensity. Moreover, the films on Ru and RuO_2 also exhibit BST(111) peak. Stronger and sharper perovskite peak of (110) from the films on Ru in comparison with those from the films deposited on other bottom electrodes implies an improved crystallinity occurred in the films on Ru. A (101) peak corresponding to RuO_2 is present in the XRD pattern of BST, indicating that an RuO_2 layer was formed at the interface between the BST and Ru during deposition. Fig. 2 depicts that the average grain size and BST(110) peak

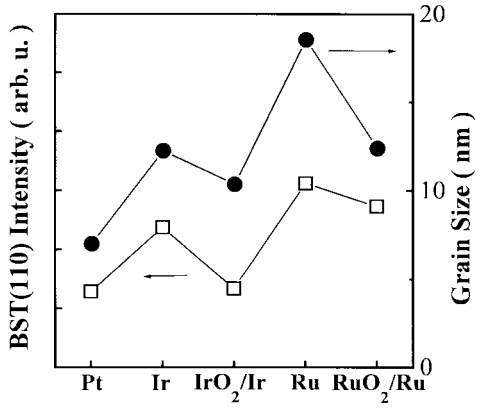

Fig. 2. Effect of bottom electrodes on the grain size and BST(110) intensity of the BST films.

intensity for the films on various bottom electrodes. The better crystallinity of BST on Ru than on other electrode materials is demonstrated by its high (110) peak intensity. The average grain size of a thin film can be estimated from full width at half maximum (FWHM) of the (110) peak in the XRD pattern by Scherrer's formula, because only the (110) peak appears clearly in all the samples. The calculated average grain size of BST deposited on Ru has a maximum value, while that of BST on Pt has the smallest value. It was confirmed that the grain size from XRD and the grain size in the direction of thickness from TEM are in fairly good agreement, for both BST films with columnar structure and those with granular structure [6]. Therefore, the grain size evaluated from XRD is suitable for helping to explain the properties of the BST thin films.

Fig. 3(a) and (b) indicates the variations of dielectric constant and loss tangent with frequency. The dielectric dispersion of BST deposited on Pt, Ir, IrO_2/Ir, Ru, and RuO_2/Ru is low (less 0.5% per decade) and these capacitors are expected to have a high charge storage density even at high frequencies. The loss tangent of BST on Pt, Ir, IrO_2/Ir, Ru, and RuO_2/Ru increases slightly with frequency. In addition, the defects in the BST films often lead to a dielectric relaxation as a function of frequency, in which the dielectric constant decreases and loss tangent increases with increasing frequency [34]. Fig. 4 shows the leakage current characteristics of the capacitors. The asymmetry of the curves implies that the leakage current is electrode-limited. The difference in work functions which are, respectively, 5.6, 5.35, and 4.8 eV for Pt, Ir, and Ru [35], and bottom electrode roughnesses, which are 1.5, 1.4, and 2.9 nm for Pt, Ir, and Ru (Fig. 5), may explain the leakage behavior of the capacitors in the positive bias. Leakage current in negative bias (gate injection) is mainly affected by the interface of BST and Pt top electrode. The greater roughness for BST films deposited on Ru compared to others (Fig. 5) may also lead to higher leakage current.

The importance of the bottom electrode in determining the root-mean-square (rms) surface roughness of the BST thin films grown on it is evident from the AFM images, as shown in Fig. 5. The greater rms surface roughness of BST on Ru and RuO_2/Ru compared to the Pt, Ir, and IrO_2/Ir may be due to the higher roughness of the Ru and RuO_2/Ru bottom electrodes

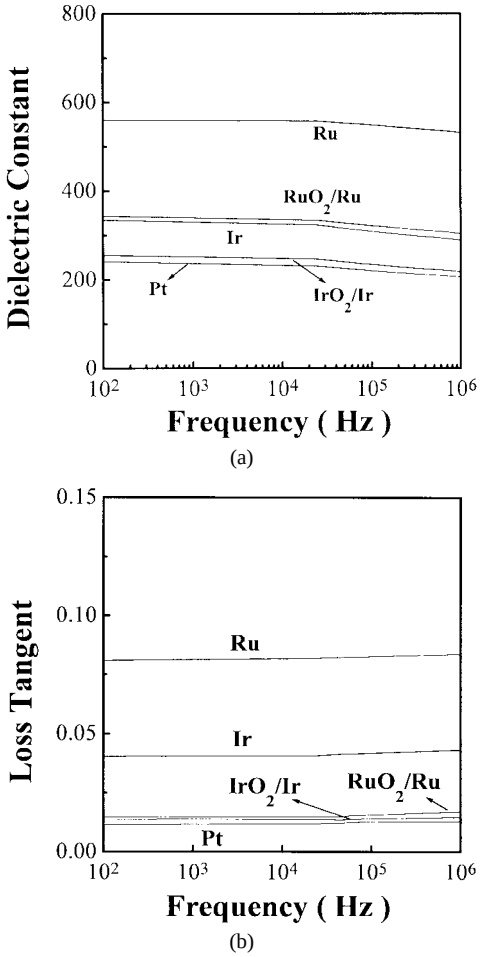

Fig. 3. Effect of frequency on (a) the dielectric constant and (b) loss tangent of BST thin films deposited on Pt, Ir, IrO_2/Ir, Ru, and RuO_2/Ru bottom electrode.

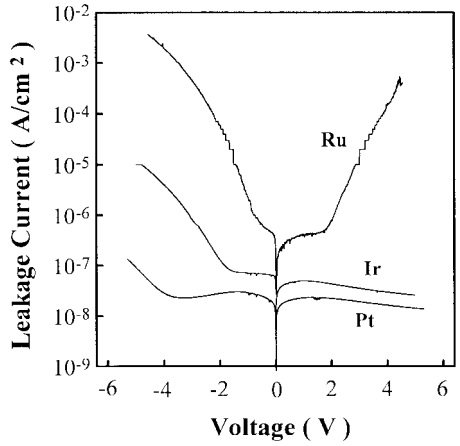

Fig. 4. Leakage current characteristics of BST capacitors on Pt, Ir, and Ru.

themselves. The grain size of the films would play an important role on the rms surface roughness of BST, the amorphous or small grain size film usually has a smooth surface. On the other hand, the surface roughness may also be affected by the number of bottom stack layers, and it mostly increases with the increase in the number of stack layers. Therefore, the rms surface roughness of BST on Ru may be attributed to both the higher roughness of the Ru bottom electrode and larger grain size

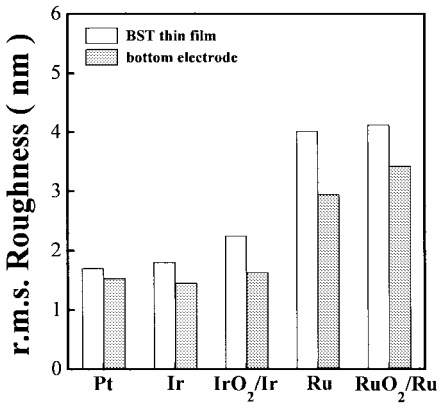

Fig. 5. RMS surface roughness of BST thin films and bottom electrodes.

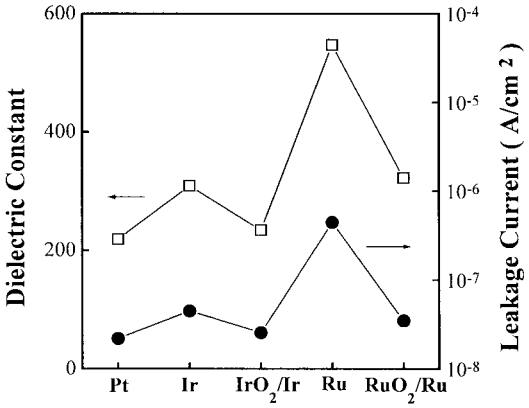

Fig. 6. Dielectric constant and leakage current of BST thin films deposited on Pt, Ir, IrO_2/Ir, Ru, and RuO_2/Ru bottom electrodes.

(Fig. 2), while that of BST on RuO_2/Ru may be due to both the higher roughness of the RuO_2/Ru bottom electrode and the effect of the number of bottom stack layers. The rms surface roughness of BST on Pt, Ir, and IrO_2/Ir mainly increases with the increase of surface roughness of the bottom electrodes, but the effect of grain size is less. Hence, the rms surface roughness of BST deposited on Ru and RuO_2/Ru is higher.

The dependence of the dielectric constant and the leakage current density (electrons transport from bottom electrode to top electrode) measured at 200 kV/cm with a delay time of 30 s on the various bottom electrodes are shown in Fig. 6. It indicates that the BST film deposited on Ru bottom electrode has a maximum dielectric constant of 548 and leakage current density of 4.4×10^{-7} A/cm^2. The BST film deposited on Pt bottom electrode has the minimum dielectric constant of 219 and leakage current density of 2.2×10^{-8} A/cm^2. The BST films can exhibit large dielectric constants due to polarization of electric dipoles. It has been reported that dielectric constant of the films was influenced by oxygen stoichiometry [13], composition [36], grain size (grain and grain boundary) [6], [29], [37], [38], crystallinity (dipole density, polarization) [6]–[8], and the space charge capacitance which may be due to space charge accumulation at the electrode interface by Schottky potential of metal electrodes [38]–[40]. In general, large grain size, good crystallinity, and small space charge capacitance width can enhance the dielectric constant of the

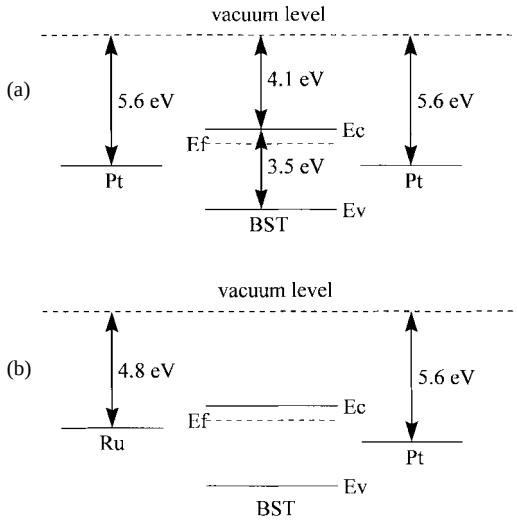

Fig. 7. Energy band situation in (a) Pt-BST-Pt, (b) Ru (bottom electrode)-BST-Pt (top electrode) system before contact.

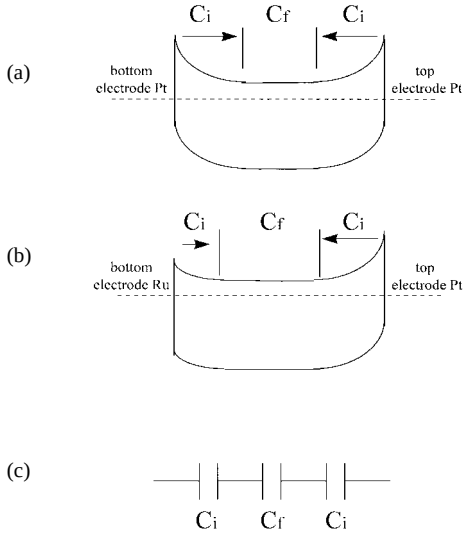

Fig. 8. Energy band diagram in (a) Pt-BST-Pt and (b) Ru (bottom electrode)-BST-Pt (top electrode) system after contact is sketched. (c) The equivalent circuit of the BST thin films.

BST films. The space charge capacitance can be affected by the metal work function and the oxygen vacancies accumulation at electrode interface. When the metal work function is large, the width of space charge capacitance will become large and the barrier height of the interface of BST/metal will become high. When the oxygen vacancies accumulate at the interface of BST/metal, the width of space charge capacitance will become small and the barrier height of the interface of BST/metal will become low. The details are illustrated in Figs. 7 and 8. The local field probably originates from the formation of space charge layers at the interface, which are located at both the top and the bottom electrode. The local field would cause lowering of the dielectric constant at the interfacial layers. The interfacial layers could be expected to work as parasitic series capacitors (C_i) with small capacitance [38] (Fig. 8). Lee reported that C_i is a low dielectric-constant capacitance [40]. Surface roughness also enlarges the capacitor electrode area,

which would be one of the factors affecting the properties of the films. However, the surface roughness of BST/RuO_2/Ru is larger than that of BST/Ir by a factor of 2.3 (Fig. 5), but the dielectric constant of BST/Ir approaches that of BST/RuO_2/Ru at approximately the same grain size and crystallinity [Figs. 2 and 3(a)]. Hence, the surface roughness effect is negligible in this study. On the other hand, the BST on Ru has the maximum grain size (the BST grains with a size of 10–100 nm, the dielectric constant increases with increase of the grain size [6], [7]) (Fig. 2), the stronger and sharper (110) peak imply an improved crystallinity (Fig. 1), and there is smaller space charge width. Hence, the BST on Ru has the maximum dielectric constant, as shown in Fig. 6. The BST on Pt has minimum grain size (Fig. 2), weaker (110) XRD peak (Fig. 1), and larger width of space charge capacitance (large work function). Hence, the BST on Pt has the minimum dielectric constant (Fig. 6). The dielectric constant of BST on Ir is between the dielectric constant of BST/Ru and BST/Pt, because the grain size (Fig. 2), (110) XRD peak intensity (Fig. 1), and work function (5.35 eV) of BST/Ir are between BST/Ru and BST/Pt. The dielectric constant of BST deposited on Ru is larger than that of BST on RuO_2/Ru, because the grain size (Fig. 2) and XRD (110) peak intensity (Fig. 1) of BST on Ru are larger than those of BST on RuO_2/Ru. For similar reasons, the dielectric constant of BST deposited on Ir is larger than that of BST on IrO_2/Ir. Hence, the grain size and crystallinity seem to play important roles in promoting the dielectric constant. The leakage current of BST thin films may be affected by the contact potential barrier. The details are illustrated in Fig. 4. The leakage current of BST deposited on RuO_2/Ru and IrO_2/Ir has the same value (as shown in Fig. 6) which indicates that their contact potential barriers are probably the same.

The breakdown field of BST on Pt, Ir, and IrO_2/Ir is around 3.5 MV/cm and on Ru and RuO_2/Ru is around 1.8 MV/cm (Table II). The difference in breakdown field between these two groups of BST films may be attributed to the different grain size and rms surface roughness between them. It is shown that the BST films on Pt, Ir, and IrO_2/Ir with smaller grain size (Fig. 2) and smooth surface (Fig. 5) show higher breakdown field, which is similar to that previously reported by Parker *et al.* [41]. Their work indicated that the smaller grain size films with higher breakdown field were obtained because they could produce more grain boundaries. On the other hand, the smooth surface can suppress the accumulation of electrons at local position, which leads to the uniform electric field, therefore, the breakdown field would also be higher. The BST on Ru with larger grain size (Fig. 2) and larger surface roughness (Fig. 5) shows lower breakdown field. However, the BST on RuO_2/Ru has smaller grain size (Fig. 2) and nearly the same surface roughness (Fig. 5) in comparison with that on Ru, but both films have near breakdown field. This inconsistent result may be due to the high surface roughness of these two films, that is, the surface roughness is the dominant factor.

The effect of bottom electrodes is summarized in Table II. We deduce a flatband model for metal-BST-metal system, the band-diagrams before contact are shown in Fig. 7(a) for the Pt-BST-Pt system where the work function of Pt is 5.6 eV and Fig. 7(b) for the Ru (bottom electrode)-BST-Pt (top electrode) system where the work function of Ru is 4.8 eV. The electron affinity of BST is assumed to be 4.1 eV and the energy bandgap is 3.5 eV [12]. Fig. 8(a) and (b) shows the energy band situation after contact for both systems in which C_f is the film-capacitance and C_i the space charge capacitance. It has been reported that C_i is a low dielectric-constant capacitance [40]. Fig. 8(c) indicates the equivalent circuit of BST thin films. Summarizing the discussion of the energy band structure of the investigated metal-BST-metal system and the experimental data of dielectric constant and leakage current, the correlation between the work function of contact material and the space charge capacitance can well explain the dependence of the dielectric constant and leakage current on various bottom electrodes, as shown in Fig. 6.

TABLE II
PROPERTIES OF THE BST THIN FILMS DEPOSITED ON VARIOUS BOTTOM ELECTRODE MATERIALS

Bottom Electrode	Pt	Ir	IrO_2/Ir	Ru	RuO_2/Ru
Dielectric Constant @100 kHz	219 (503)	309 (593)	234 (501)	548 (325)	322 (433)
Leakage Current (10^{-8} A/cm^2) @200 kV/cm	2.2 (2.5)	4.5 (1.9)	2.5 (3.3)	44 (2.1)	3.5 (2.4)
Loss Tangent @100 kHz	0.014 (0.015)	0.046 (0.019)	0.016 (0.02)	0.083 (0.019)	0.017 (0.012)
Work Function (eV)	5.6	5.35	*	4.8	*
Breakdown Field (MV/cm)	3.84	3.68	3.49	1.94	1.84
Fatigue Endurance (cycling number)	$>10^{11}$	$>10^{11}$	$>10^{11}$	$>10^{11}$	$>10^{11}$
BST Surface Roughness (nm)	1.7	1.8	2.25	4.02	4.12
Stability in O_2 ambient	up to 700 ℃	up to 700 ℃	up to 700 ℃	up to 500 ℃	up to 700 ℃

( ) : 700 ℃, O_2 annealing for 20 min

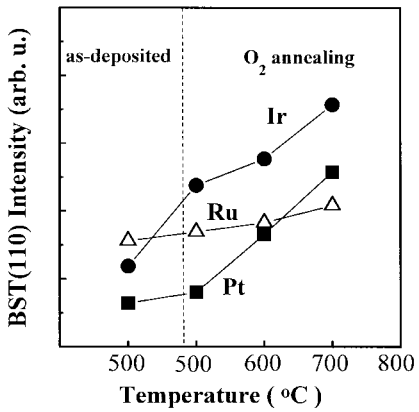

Fig. 9. BST(110) intensity of BST films deposited at 500 °C on Pt, Ir, and Ru and afterward annealed for 20 min at 500, 600, and 700 °C in O_2 ambient.

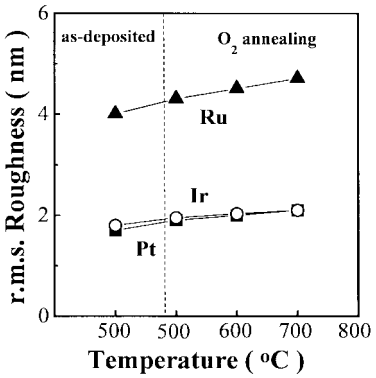

Fig. 10. Surface roughness of BST films deposited at 500 °C on Pt, Ir, and Ru and afterward annealed for 20 min at 500, 600, and 700 °C in O_2 ambient.

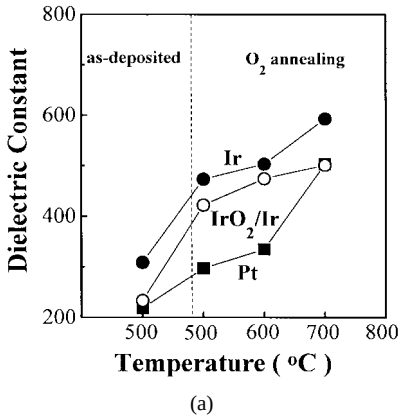

(a)

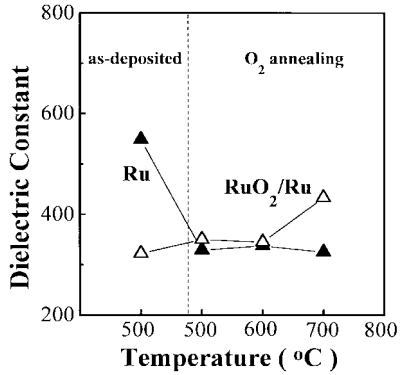

(b)

Fig. 11. Dielectric constant of BST films deposited at 500 °C on (a) Pt, Ir, and IrO_2/Ir and (b) Ru and RuO_2/Ru and afterward annealed for 20 min at 500, 600, and 700 °C in O_2 ambient.

B. Effect of Annealing in O_2 Ambient

Fig. 9 depicts that the BST(110) peak intensity for the BST films deposited on Pt, Ir, and Ru at 500 °C and afterward FN annealed at 500, 600, and 700 °C in O_2 ambient for 20 min. The (110) diffraction peak of the BST films increases with increasing annealing temperature. The results of XRD suggest that an improvement of the crystallinity of BST films can be achieved by annealing treatment. Fig. 10 depicts that the surface roughness of BST thin films deposited on Pt, Ir, and Ru at 500 °C and afterward FN annealed at 500, 600, and 700 °C in O_2 ambient for 20 min. The surface roughness of BST films increases with increasing annealing temperature. The surface roughness effect was considered to be negligible in this study, which was illustrated in Fig. 6.

Fig. 11(a) shows that the variation of dielectric constant of BST thin films, deposited on Pt, Ir, and IrO_2/Ir bottom electrodes at 500 °C and sequentially annealed in O_2 at 500, 600, and 700 °C for 20 min. The dielectric constant increases with increasing the annealing temperature because the intensities of the XRD peaks of BST on Pt and Ir increase with increasing annealing temperature (Fig. 9). Fig. 11(b) shows that the dielectric constant of BST films, deposited on Ru and RuO_2/Ru bottom electrodes at 500 °C and afterward annealed for 20 min at 500, 600, and 700 °C in O_2 ambient is dependent on the postannealing temperature. The dielectric constant of BST on RuO_2/Ru increases with increasing the annealing temperature, while that of BST on Ru decreases with increasing the annealing temperature. Hence, the BST deposited on Pt, Ir, IrO_2/Ir, and RuO_2/Ru after postannealing are more stable than that on Ru.

From SIMS data, we observed that the oxygen concentration at the BST/Ru interface is larger than the oxygen concentration at BST/Pt and BST/Ir interfaces, as shown in Fig. 12(a)–(c). The BST/Ru interface may be oxidized during deposition and form a thin transition-metal-oxide-layer. The XRD data shows the RuO_2(101) peak of BST on Ru (Fig. 1) and a thin RuO_2 layer was formed at the interface between the BST and Ru during deposition. Hence, the interfaces of BST/Ru may suppress the accumulation of oxygen vacancies. Fig. 13(a)–(c) indicates that the SIMS data of the BST deposited on Pt, Ir, and Ru and afterward annealed in O_2 at 600 °C for 20 min. For understanding the effect of annealing on the dielectric properties of the BST on various bottom electrodes, we compare SIMS data of BST films before and after annealing (Figs. 12 and 13). There is no change in the Ti, Pt, and O concentration profiles at the interface of BST/Pt after annealing, as indicated in Figs. 12(a) and 13(a). The Ti and Ir profiles of BST on Ir remain the same, but the oxygen concentration at the interface slightly increases [Figs. 12(b) and 13(b)], that is, an IrO_2 layer is probably formed. No change in the leakage current at 200 kV/cm happens in BST on Pt after postannealing, while the leakage current of

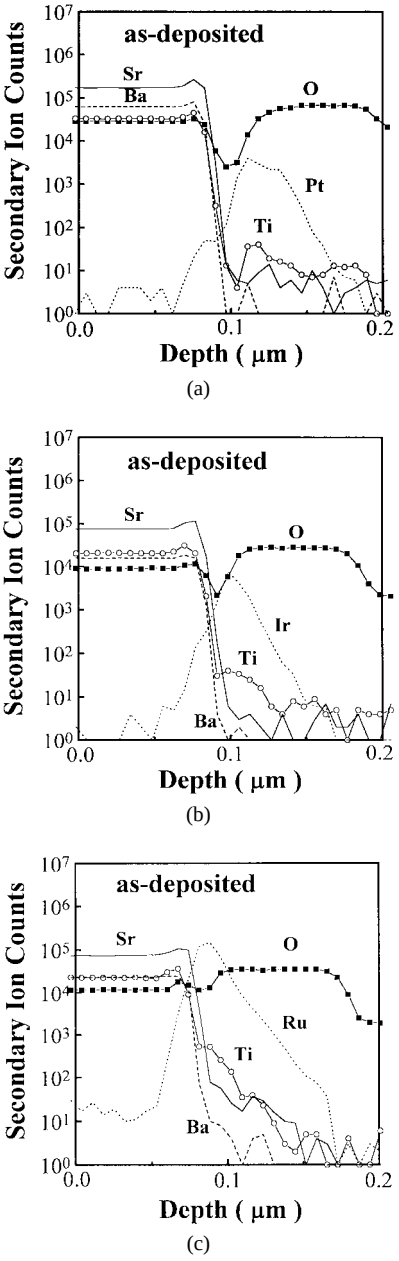

Fig. 12. SIMS profile of BST as-deposited on (a) Pt annealing, (b) Ir bottom electrodes, and (c) Ru bottom electrodes.

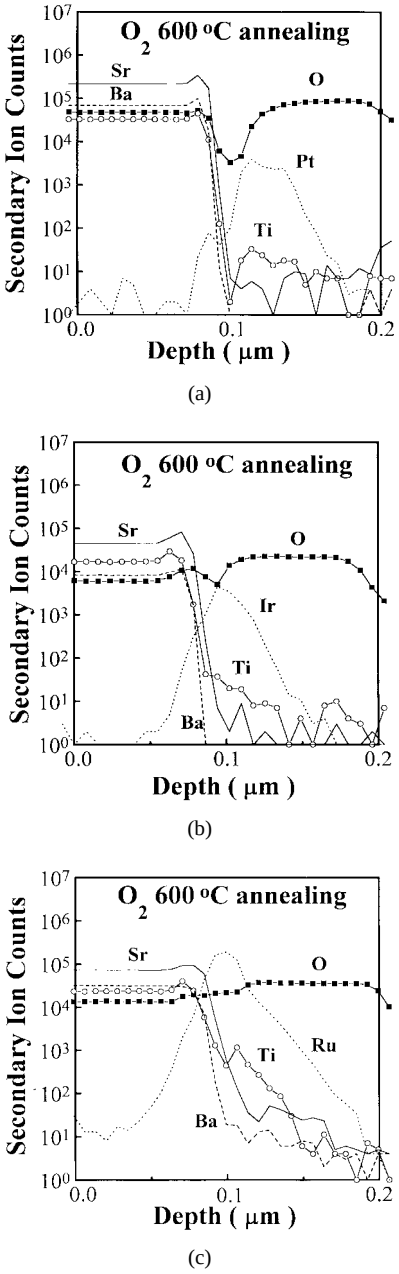

Fig. 13. SIMS profile of BST deposited on (a) Pt after 600 °C, O_2 annealing, (b) Ir after 600 °C, O_2 annealing, and (c) Ru after 600 °C, O_2 annealing.

BST on Ir after postannealing decrease with the annealing temperature (Fig. 14). It is indicated in Figs. 12(c) and 13(c) that changes in the Ti and Ru profiles of BST on Ru occur and the oxygen concentration at the interface increases due to annealing. A thin interfacial layer of RuO_2 at BST/Ru was formed during deposition (Fig. 1), and this layer becomes thicker after annealing (XRD data indicates the RuO_2(101) peak is stronger after annealing). This change leads to the leakage current of BST on Ru after postannealing approaches to that on RuO_2/Ru (Figs. 6 and 14). The large change in the dielectric constant is also attributed to a possible thin interfacial layer like (Ba, Sr)(Ru, Ti)O_3 formed at BST/Ru by the interdiffusion of those ions after annealing, because of the similarity of the ionic radii of Ru^{+4} and Ti^{+4}, as shown in Fig. 11(b). On a separate study, we found that the (Ba, Sr)(Ru,

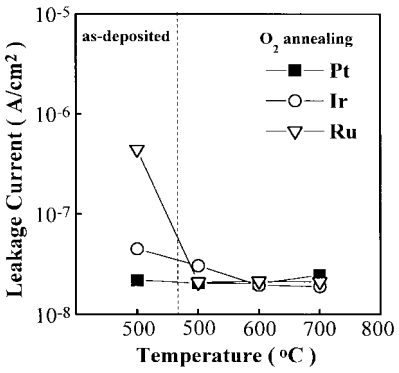

Fig. 14. Leakage current of BST films deposited at 500 °C on Pt, Ir, and Ru and afterward annealed for 20 min at 500, 600, and 700 °C in O_2 ambient.

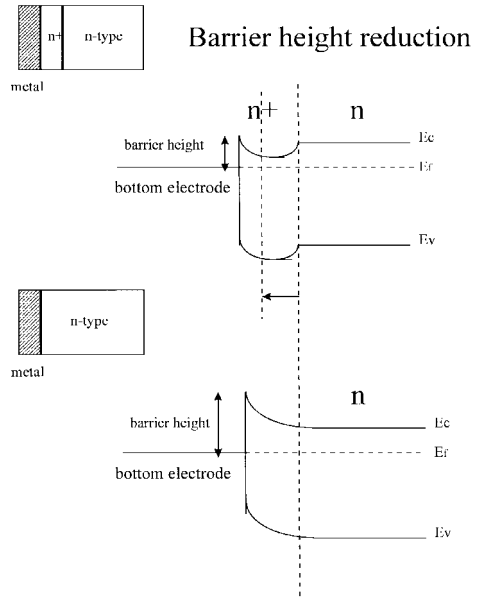

Fig. 15. Barrier height of metal n^+-type–n type and metal n-type structures.

Ti)O_3 bulk is a low dielectric constant material. The interfaces of BST on IrO_2/Ir and RuO_2/Ru after postannealing are stable, similar to the BST on Pt and Ir.

Fig. 15 is provided for further explaining the effect of the change in the interface due to annealing on the properties of BST films. The thinner interfacial layers of IrO_2 and RuO_2 are suggested to suppress the accumulation of the oxygen vacancies at the BST/Ru and BST/Ir interfaces. Therefore, the interface of the BST/Ru and BST/Ir has reduced accumulation of oxygen vacancies after postannealing. The BST film tends to show an n-type conductivity because the oxygen vacancy acts as a donor dopant. The higher concentration of oxygen vacancy accumulated at the interface tends to show an n^+-type conductivity (Fig. 15). Hence, the BST/Ru and BST/Ir structures before postannealing are similar to the "n-type-n^+-type metal" structure, whereas those after postannealing are similar to the "n-type metal" structure. On the basis of the point of view of the physics of semiconductor devices, the n-type–n^+-type metal structure will result in barrier height reduction, which leads to larger barrier height occurred in the n-type metal structure, as shown in Fig. 15. Therefore, the leakage current of BST on Ir and Ru after postannealing decreases with the annealing temperature, because the barrier height of BST on Ir and Ru after postannealing increases with the annealing temperature.

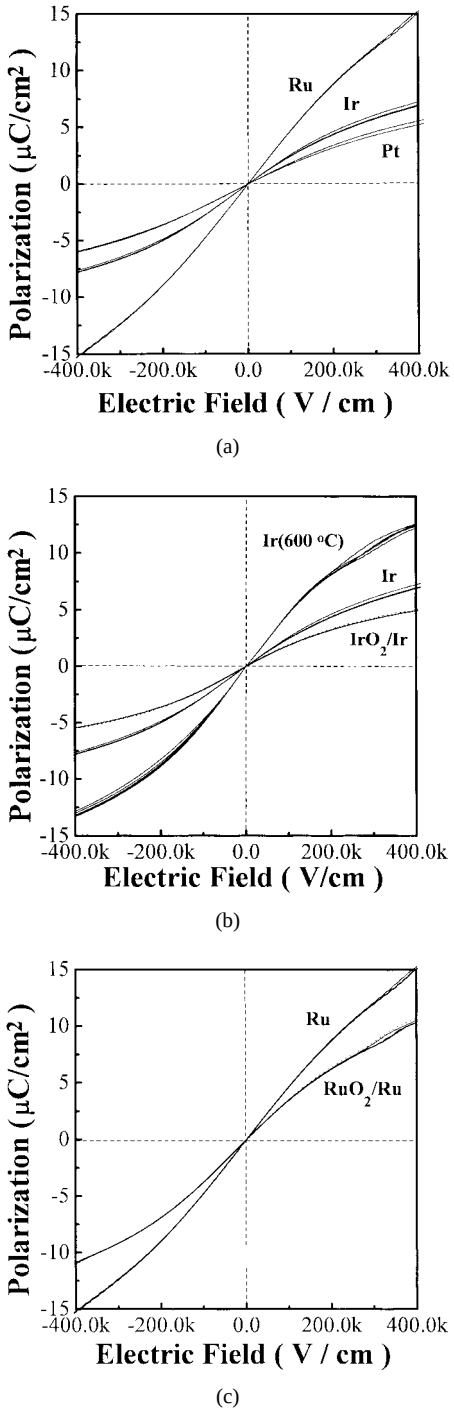

Fig. 16. Polarization versus electric field of BST films deposited on (a) Pt, Ir, and Ru, (b) Ir, Ir (600 °C) and IrO_2/Ir, and (c) Ru and RuO_2/Ru.

C. Reliability

The paraelectric perovskite phase of BST over the device operating temperature shows that it does not exhibit fatigue. Because of the large variations in material characteristics that take place at T_c, it is desirable to use a material with a transition temperature lower than the normal temperature range of DRAM operation: 0–70 °C ambient and 0–100 °C on chip [4], [9]. Fig. 16(a)–(c) shows that the 80-nm thick BST films deposited at 500 °C with various bottom electrodes are linear from experimental data of polarization versus electric field. The film deposited on Ru at 500 °C has a charge storage density of 49 fC/μm^2 at an applied field of 100 kV/cm. And the BST film deposited on Ir at 500 °C and annealed at O_2 600 °C for 20 min has a charge storage density of 47 fC/μm^2 at an applied field of 100 kV/cm. The polarization of the films may be enhanced in BST films deposited on the Ir bottom electrode after postannealing. It demonstrates an extremely thin polarization voltage loop. This thin polarization loop could lead to a low energy dissipation during switching. Fig. 17 depicts the endurance data of BST films. The samples

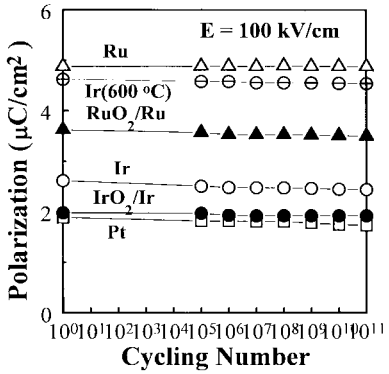

Fig. 17. Polarization of BST films deposited on Pt, Ir, Ir (600 °C), IrO_2/Ir, Ru, and RuO_2/Ru versus cycle number at 100 kV/cm.

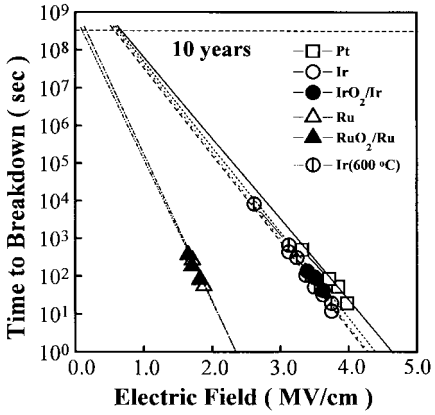

Fig. 18. Time to breakdown of the BST films on various bottom electrodes as a function of stress field.

exhibit very little degradation of polarization at ±3 V square wave after 10^{11} cycles. These results confirm that the sputtered BST films do not experience any fatigue problem which was commonly observed in PZT films. The effect of bottom electrodes is summarized in Table II. Lifetime extrapolation using constant voltage stress time-dependent dielectric breakdown studies (Fig. 18) predicts the ten-year lifetime at 2 V operating voltage. It indicates that the BST on Pt, Ir, Ir (600 °C) (BST annealed at O_2 600 °C for 20 min) and IrO_2/Ir samples have a longer lifetime at 2 V operating voltage than the BST on Ru and RuO_2/Ru samples.

IV. Conclusions

The crystallinity and electrical properties of BST films deposited on Pt, Ir, IrO_2/Ir, Ru, and RuO_2/Ru bottom electrodes strongly depend on the postannealing process after deposition. We have shown that BST thin film, deposited on Ru at 500 °C, has the dielectric constant of 548, a loss tangent of 0.083 at 100 kHz, a leakage current of 4.4×10^{-7} A/cm^2 at an electric field of 200 kV/cm with a delay time of 30 s, and a charge storage density of 49 fC/μm^2 at an applied field of 100 kV/cm. And such film after annealing in O_2 at 700 °C for 20 min reduces the leakage current to 2.1×10^{-8} A/cm^2 at an electric field of 200 kV/cm with a delay time of 30 s and lowers the dielectric constant to 325. The BST film deposited on Ir at 500 °C after 700 °C annealing in O_2 for 20 min has the dielectric constant of 593, a loss tangent of 0.019 at 100 kHz, a leakage current of 1.9×10^{-8} A/cm^2 at an electric field of 200 kV/cm with a delay time of 30 s, and a charge storage density of 53 fC/μm^2 at an applied field of 100 kV/cm. On the basis of the measurement results, the BST films on Ir with postannealing can obtain better dielectric properties than on other bottom electrodes.

We have demonstrated that the bottom electrodes appear to have a strong influence on the degradation and breakdown properties of the BST thin films. The BST film deposited on Ru has faster degradation than those deposited on Pt, Ir, and Ir (600 °C). The ten-year lifetime of time-dependent dielectric breakdown (TDDB) studies indicate that BST films on Pt, Ir IrO_2/Ir, and Ir (600 °C) have longer lifetimes at 2 V operating voltage than those on Ru and RuO_2/Ru. The longest lifetime occurred in the BST film on Pt was ascribed to smaller grain size, higher Schottky barrier, and less polarization-enhanced electron transport in the film on Pt.

References

[1] Y. Ohno, T. Horikawa, H. Shinkawata, K. Kashihara, T. Kuroiwa, T. Okudaira, Y. Hashizume, K. Fukumoto, T. Eimori, T. Shibano, K. Arimoto, H. Itoh, T. Nishimura, and H. Miyoshi, "A memory cell capacitor with $Ba_xSr_{1-x}TiO_3$ (BST) film for advanced DRAM's," in *Symp. VLSI Technology, Dig. Tech. Papers*, 1994, pp. 149–150.

[2] T. Eimori, Y. Ohno, J. Matsufusa, S. Kishimura, A. Yoshida, H. Sumitani, T. Maruyama, Y. Hayashide, K. Moriizumi, T. Katayama, M. Asakura, T. Horikawa, T. Shibano, H. Itoh, K. Namba, T. Nishimura, S. Satoh, and H. Miyoshi, "A newly designed planar stacked capacitor cell with high dielectric constant film for 256 Mbit DRAM," in *IEDM Tech. Dig.*, 1993, pp. 631–634.

[3] E. Fujii, Y. Uemoto, S. Hayashi, T. Nasu, Y. Shimada, A. Matsuda, M. Kibe, M. Azuma, T. Otsuki, G. Kano, M. Scott, L. D. Mcmillan, and C. A. Paz de Araujo, "ULSI DRAM technology with $Ba_{0.7}Sr_{0.3}TiO_3$ film of 1.3 nm equivalent SiO_2 thickness and 10^{-9} (A/cm^2) leakage current," in *IEDM Tech. Dig.*, 1992, pp. 267–270.

[4] K. Koyama, T. Sakuma, S. Yamamichi, H. Watanabe, H. Aoki, S. Ohya, Y. Miyasaka, and T. Kikkawa, "A stacked capacitor with $Ba_xSr_{1-x}TiO_3$ for 256 M DRAM," in *IEDM Tech. Dig.*, 1991, pp. 823–826.

[5] H. N. A. Shareef, O. Auciello, and A. I. Kingon, "Electrical properties of ferroelectric thin film capacitors with hybrid (Pt, RuO_2) electrodes for nonvolatile memory applications," *J. Appl. Phys.*, vol. 77, no. 5, pp. 2146–2154, 1995.

[6] T. Horikawa, N. Mikami, T. Makita, J. Tanimura, M. Kataoka, K. Sato, and M. Nunoshita, "Dielectric properties of (Ba, Sr)TiO_3 thin film deposited by RF sputtering," *Jpn. J. Appl. Phys.*, vol. 32, pp. 4126–4130, 1993.

[7] T. Kuoiwa, Y. Tsunenine, T. Horikawa, T. Makita, J. Tanimura, N. Mikami, and K. Sato, "Dielectric properties of $(Ba_xSr_{1-x})TiO_3$ thin films prepared by RF sputtering for dynamic random access memory application," *Jpn. J. Appl. Phys.*, vol. 33, pp. 5187–5191, 1994.

[8] R. Khamankar, B. Jiang, R. Tsu, W. Y. Hsu, J. Nulman, S. Summerfelt, and M. Anthony, and J. Lee, "A novel low-temperature process for high dielectric constant BST thin films for ULSI DRAM applications," in *Symp. VLSI Technology Dig. Tech. Papers*, 1995, pp. 127–128.

[9] S. G. Yoon and A. Safari, "$(Ba_{0.5},Sr_{0.5})TiO_3$ thin film preparation by RF magnetron sputtering and its electric properties," *Thin Solid Films*, vol. 254, pp. 211–215, 1995.

[10] S. O. Park, C. S. Hwang, H. J. Cho, C. S. Kang, H. K. Kang, S. I. Lee, and M. Y. Lee, "Fabrication and electrical characterization of Pt/(Ba, Sr)TiO_3/Pt capacitors for ultralarge-scale integrated DRAM applications," *Jpn. J. Appl. Phys.*, vol. 35, pp. 1548–1552, 1996.

[11] M. S. Tsai, S. C. Sun, and T. Y. Tseng, "Effect of oxygen to argon ratio on properties of (Ba, Sr)TiO_3 thin films prepared by radio-frequency magnetron sputtering." *J. Appl. Phys.*, vol. 82, no. 7, pp. 3482–3487, 1997.

[12] H. Kobayashi and T. Kobayashi, "Heteroepitaxial growth of quaternary $Ba_xSr_{1-x}TiO_3$ thin films by ArF excimer laser ablation," *Jpn. J. Appl. Phys.*, vol. 33, pp. L533–L536, 1994.

[13] A. Yuuki, M. Yamamuka, T. Makita, T. Horikawa, T. Shibano, N. Hirano, H. Maeda, N. Mikami, K. Ono, H. Ogata, and H. Abe, "Novel stacked capacitor technology for 1 Gbit DRAM's with CVD-(Ba,Sr)TiO_3 thin films on a thick storage node of Ru," in *IEDM Tech. Dig.*, 1995, pp. 115–118.
[14] K. Takemura, S. Yamamichi, P. Y. Lesaicherre, K. Tokashiki, H. Miyamoto, H. Ono, Y. Miyasaka, and M. Yoshida, "RuO_2/TiN based storage electrodes for (Ba, Sr)TiO_3 dynamic random access memoery capacitors," *Jpn. J. Appl. Phys.*, vol. 34, pp. 5224–5229, 1995.
[15] T. Sakuma, S. Yamamichi, S. Matsubara, H. Yamaguchi, and Y. Miyasaka, "Barrier layers for realization of high capacitance density in $SrTiO_3$ thin film capacitor on silicon," *Appl. Phys. Lett.*, vol. 57, pp. 2431–2433, 1990.
[16] R. Khamankar, B. Jiang, R. Tsu, W. Y. Hsu, J. Nulman, S. Summerfelt, M. Anthony, and J. Lee, "A novel low temperature process for high dielectric constant BST thin films for ULSI DRAM applications," in *1995 Symp. VLSI Technology Dig. Tech. Papers*, pp. 127–128.
[17] T. S. Chen, D. Hadad, V. Balu, B. Jiang, S. H. Kuah, P. C. Mcintypre, S. R. Summerfelt, J. M. Anthony, and J. C. Lee, "Ir-electroded BST thin film capacitors for 1 giga-bit DRAM application," in *IEDM Tech. Dig.*, vol. 27.2.1, 1996, pp. 679–682.
[18] V. Balu, T. S. Chen, B. Jiang, D. Hadad, S. H. Kuah, S. Katakam, B. White, B. Melnick, P. Chu, R. E. Jones, S. J. Gillespie, and J. C. Lee, "A bi-layer Pt/Ir electrode system for barium strontium titanate (BST) thin film capacitors for high density memory applications," in *IEDM Tech. Dig.*, 1997, pp. 145–146.
[19] H. Yamaguchi, T. Iizuka, H. Koga, K. Takemura, S. Sone, H. Yabuta, S. Yamamichi, P. Y. Lesaicherre, M. Suzuki, Y. Kojima, K. Nakajima, N. Kasai, T. Sakuma, Y. Kato, Y. Miyasaka, M. Yoshida, and S. Nishimoto, "A stacked capacitor with an MOCVD-(Ba, Sr)TiO_3 film and RuO_2/Ru storage node on a TiN-capped plug for 4-Gbit DRAM's and beyond," in *IEDM Tech. Dig.*, vol. 27.1.1, 1996, pp. 675–678.
[20] K. Takemura, T. Sakuma, and Y. Miyasaka, "High dielectric constant (Ba, Sr)TiO_3 thin films prepared on RuO_2/sapphire," *Appl. Phys. Lett.*, pp. 2967–2969, 1994.
[21] K. Hong, H. J. Sun, and Y. S. Yu, "Thermal stability of RuO_2/Ru-based storage node for DRAM application," *ULSI Metallization*, pp. 192–193, 1998.
[22] ———, "Electrical properties of BST films deposited on Ir and IrO_2 electrode as a DRAM capacitor," *ULSI Metallization*, pp. 190–191, 1998.
[23] S. Yamamichi, P. Y. Lesaicherre, H. Yamaguchi, K. Takemura, S. Sone, H. Yabuta, K. Sato, T. Tamura, K. Nakajima, S. Ohnishi, K. Tokashiki, Y. Hayashi, Y. Kato, Y. Miyasaka, M. Yoshida, and H. Ono, "A stacked capacitor technology with ECR plasma MOCVD (Ba, Sr)TiO_3 and RuO_2/Ru/TiN/Ti six storage nodes for Gb-Scale DRAM's," *IEEE Trans. Electron Devices*, vol. 44, no. 7, pp. 1076–1081, 1997.
[24] C. S. Hwang, B. T. Lee, H. J. Cho, K. H. Lee, C. S. Kang, H. Hideki, S. I. Lee, and M. Y. Lee, "A positive temperature coefficient of resistivity effect from a paraelectric Pt/($Ba_{0.5}$,$Sr_{0.5}$)TiO_3/IrO_2 thin film capacitor," *Appl. Phys. Lett.*, vol. 71, no. 3, pp. 371–373, 1997.
[25] H. J. Cho, C. S. Kang, C. S. Hwang, J. W. Kim, H. Horh, B. T. Lee, S. I. Lee, and M. Y. Lee, "Structural and electrical properties of $Ba_{0.5}Sr_{0.5}TiO_3$ films on Ir and IrO_2 electrodes," *Jpn. J. Appl. Phys.*, vol. 36, part 2, no. 7A, pp. L874–L876, 1997.
[26] T. Kawahara, M. Yamamuka, J. Tanimura, M. Tarutani, T. Kuroiwa, T. Horikawa, and K. Ono, "Influence of buffer layers and barrier metals on properties of (Ba, Sr)TiO_3 films prepared by liquid source chemical vapor deposition," *Jpn. J. Appl. Phys.*, vol. 36, part 1, no. 9B, pp. 5874–5878, 1997.
[27] S. Yamamichi, A. Yamamichi, D. Park, and C. Hu, "Impact of time dependent dielectric breakdown and stress induced leakage current on the reliability of (Ba, Sr)TiO_3 thin film capacitors for Gbit-scale DRAM's," in *IEDM Tech. Dig.*, vol. 10-5, 1997, pp. 188–191.
[28] Y. Fukuda, K. Numata, K. Aoki, and A. Nishimura, "Origin of dielectric relaxation observed for $Ba_{0.5}Sr_{0.5}TiO_3$ thin film capacitor," *Jpn. J. Appl. Phys.*, vol. 35, pp. 5178–5180, 1996.
[29] C. S. Hwang, S. O. Park, H. J. Cho, C. S. Kang, H. K. Kang, S. I. Lee, and M. Y. Lee, "Deposition of extremely thin (Ba, Sr)TiO_3 thin films for ultra large scale integrated dynamic random access memory application," *Appl. Phys. Lett.*, vol. 67, pp. 2819–2821, 1995.
[30] N. Ichinose and T. Ogiwara, "Preparation and rapid thermal annealing effect of (Ba, Sr)TiO_3 thin films," *Jpn. J. Appl. Phys.*, vol. 34, pp. 5198–5201, 1995.
[31] T. S. Chen, V. Balu, B. Jiang, S. H. Kuah, J. C. Lee, P. Chu, R. E. Jones, P. Zurcher, D. J. Taylor, and S. Gillespie, "Stability of reactive DC-sputtered Ir and IrO_2 thin films in various ambients," *Integrated Ferroelectrics*, vol. 16, pp. 191–198, 1997.
[32] A. Grill, W. Kane, J. Viggiano, M. Brady, and R. Laibowitz, "Base electrodes for high dielectric constant oxide materials in silicon technology," *J. Mater. Res.*, vol. 7, no. 12, pp. 3260–3265, 1992.
[33] B. Jiang, V. Balu, T. S. Chen, S. H. Kuah, J. C. Lee, P. Y. Chu, R. E. Jones, P. Zurcher, D. J. Taylor, M. L. Kottke, and S. J. Gillespie, "A new electrode technology for high density nonvolatile ferroelectric $SrBi_2Ta_2O_9$ memories," in *Symp. VLSI Technology Dig. Tech. Papers*, 1996, pp. 26–27.
[34] M. S. Tsai and T. Y. Tseng, "Effect of bottom electrodes on dielectric relaxation and defect analysis of ($Ba_{0.47}Sr_{0.53}$)TiO_3 thin film capacitors," *Mat. Chem., Phys.*, vol. 57, pp. 47–56, 1998.
[35] S. M. Sze, *Phys. of Semiconductor Devices*, 2nd ed. New York: Wiley, 1981, p. 251.
[36] K. Abe and S. Komatsu, "Ferroelectric properties in epitaxially grown $Ba_xSr_{1-x}TiO_3$ thin films," *J. Appl. Phys.*, vol. 77, pp. 6461–6465, 1995.
[37] T. Horikawa, N. Mikami, H. Ito, Y. Ohno, T. Makita, and K. Sato, "$Ba_{0.75}Sr_{0.25}TiO_3$ films for 256 Mbit DRAM," *IEICE Trans. Electron.*, vol. E77-C, pp. 385–390, 1994.
[38] K. Abe and S. Komatsu, "Epitaxial growth and dielectric properties of $Ba_{0.24}Sr_{0.76}TiO_3$ thin film," *Jpn. J. Appl. Phys.*, vol. 33, pp. 5297–5300, 1994.
[39] P. Bhattacharya, K. H. Park, and Y. Nishhioka, "Control of grain structure of laser-deposited (Ba, Sr)TiO_3 films to reduce leakage current," *Jpn. J. Appl. Phys.*, vol. 33, pp. 5231–5234, 1994.
[40] J. J. Lee, C. L. Thio, and S. B. Desu, "Electrode contacts on ferroelectric Pb(Zr_xTi_{1-x})O_3 and $SrBi_2Ta_2O_9$ thin films and their influence on fatigue properties," *J. Appl. Phys.*, vol. 78, pp. 5073–5078, 1995.
[41] L. H. Parker and A. F. Tasch, "Ferroelectric material for 64 Mb DRAM's," *IEEE Circuits Devices Mag.*, pp. 17–26, 1990.

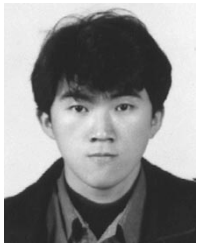

Ming Shiahn Tsai was born in Tainan, Taiwan, R.O.C., on October 19, 1971. He received the B.S. degree from the Department of Electrical Engineering, National Tsing Hua University, Hsinchu, Taiwan, in 1994, and the M.S. degree from National Chiao Tung University, Hsinchu, Taiwan, in 1996. He is currently pursuing the Ph.D. degree at the Institute of Electronics, National Chiao Tung University.

His research interests are high dielectric constant materials, ferroelectric materials, dielectric film reliability, and defects analysis.

S. C. Sun, photograph and biography not available at the time of publication.

Tseung-Yuen Tseng (SM'94) received the Ph.D. degree in electro-ceramics from the School of Materials Engineering, Purdue University, West Lafayette, IN, in 1982.

Before joining National Chiao-Tung University, Hsinchu, Taiwan, R.O.C., in 1983, where he is now a Professor in the Department of Electronics Engineering and the Institute of Electronics, he was briefly associated with the University of Florida. His professional interests are electronic ceramics, ceramic sensors, high-temperature superconductors, and ferroelectric thin films. He has published over 200 research papers.

Dr. Tseng is a Fellow of the American Ceramic Society. He has received several awards including a Distinguished Research Award from the National Science Council of the Republic of China and the Ceramic Medal from the Chinese Ceramic Society.